Available online at www.sciencedirect.com
ScienceDirect
Catalysis Today 129 (2007) 414–420
CATALYSIS TODAY
www.elsevier.com/locate/cattod

Hydrothermal synthesis, characterization, and photocatalytic performances of Cr incorporated, and Cr and Ti co-incorporated MCM-41 as visible light photocatalysts for water splitting

Shaohua Shen, Liejin Guo *

State Key Laboratory of Multiphase Flow in Power Engineering, Xi'an Jiaotong University, Xi'an 710049, PR China

Available online 21 September 2007

Abstract

A series of Cr incorporated, and Cr and Ti co-incorporated MCM-41 photocatalysts were synthesized by hydrothermal method. X-ray diffraction (XRD), UV–vis diffuse reflectance spectra (UV–vis), Fourier transform infrared spectroscopy (FTIR), X-ray fluorescence analysis (XRF), N_2 adsorption–desorption isotherms and Raman spectra were used to investigate the effects of the incorporated elements on the structure of MCM-41. The experimental results for photocatalytic water splitting under visible light irradiation ($\lambda > 430$ nm) demonstrated that the photocatalytic activities of Cr-MCM-41 and Cr-Ti-MCM-41 catalysts for hydrogen production decreased with an increase in the amount of Cr incorporated. Compared with the Cr-MCM-41 which had the same amount of incorporated Cr, the Cr-Ti-MCM-41 exhibited much higher hydrogen evolution activities.

Keywords: Incorporated MCM-41; Photocatalyst; Hydrogen evolution; Visible light

1. Introduction

Hydrogen is one of the most important chemicals in the industrial commodity. Hydrogen is mainly consumed in the hydrotreating and synthesis of ammonia, methanol, higher alcohols and aldehydes processes. Generation of hydrogen via photocatalytic decomposition of water has attracted a lot of attention from the viewpoint of conversion of solar energy into chemical fuels.

Recently, photocatalytic formation of hydrogen and oxygen on semiconductors such as TiO_2 [1,2], $SrTiO_3$ [3] and ZrO_2 [4] has been widely investigated. However, these semiconductor photocatalysts possess a very low efficiency in the formation of photoexcited charge that is transferred to the surfaces to initiate the decomposition of H_2O.

Since the invention of M41S mesoporous molecular sieves [5,6], much attention has been paid to the mesoporous silicate materials. Recently, mesoporous silicate materials involving transition-metal ions within the mesoporous framework have opened new possibilities in many research areas not only for catalysis but also for various photochemical processes, such as photocatalytic degradation of organic pollutant [7–9], water splitting for hydrogen evolution [10] and so on. However, to the best of our knowledge, it has not been reported that transition-metal ions incorporated mesoporous silicate materials show stable photocatalytic activity for water reduction and oxidation under visible light irradiation. Here we reported a series of Cr incorporated and Cr, Ti co-incorporated MCM-41 synthesized by a simple hydrothermal method, and the tests of photocatalytic activity imply that transition-metal ions incorporated mesoporous silicate materials could be a new class of stable visible-light sensitive photocatalyst for water reduction.

2. Experimental

2.1. Synthesis of Cr incorporated and Cr, Ti co-incorporated MCM-41

The photocatalysts of Cr incorporated and Cr, Ti co-incorporated MCM-41 were prepared according to the literature [11] using the cationic surfactant cetyltrimethylammonium bromide (CTAB) as a template and

* Corresponding author. Tel.: +86 29 82663895; fax: +86 29 82669033.
E-mail address: lj-guo@mail.xjtu.edu.cn (L. Guo).

0920-5861/$ – see front matter © 2007 Elsevier B.V. All rights reserved.
doi:10.1016/j.cattod.2006.08.070

tetrathyorthosilicate (TEOS) as silicon source in basic conditions by a direct hydrothermal synthesis method. For Cr(x)-MCM-41 synthesis, the final gel has a molar composition of CTAB:TEOS:NaOH:$Cr(NO_3)_3$:H_2O = 1:7.5x/(1 + x):1.8:7.5/(1 + x):500, the symbol x (= 100, 50, 25, 10) represented the mole rate of Si to Cr. Synthesis of Cr(x)-MCM-41 (x = 100) was carried out as follows: at 40 °C, 1.82 g of CTAB was dissolved into a solution containing 45 mL of deionized water and 0.42 g of NaOH, then 8.21 mL of TEOS was added dropwise to the above solution and stirred vigorously for 1 h for hydrolysis of TEOS. The resulting sol was stirred and 0.75 mL of 0.5 M $Cr(NO_3)_3$ aqueous solution was added followed by pH adjustment to 10.5–11.0 using NaOH aqueous solution. Finally the mixture was stirred at 40 °C for another 1 h, the resulting gel was transferred to a 90-mL Teflon-lined autoclave and held at 100 °C for 3 days. The product obtained was filtered, washed with water, and dried in air at 100 °C overnight. To remove the surfactant, the samples were calcined in air at 500 °C for 5 h at a heating rate of 2 °C/min.

For Cr(x)-Ti-MCM-41 (x = 100, 50, 25, 10) synthesis, the process was the same, except that 0.374 g of tetrabutyl titanate (TBOT) was added dropwise into the sol after the addition of TEOS. In all the Cr(x)-Ti-MCM-41 samples, the mole ratio of Ti:Si is 0.03; while for pure MCM-41 synthesis, neither TBOT nor $Cr(NO_3)_3$ aqueous solution was added.

As reference, TiO_2 loaded Cr-MCM-41 was also synthesized as follows: at room temperature, 1 g of prepared Cr-MCM-41 was added into 20 mL of TBOT ethanol solution (0.025 mol L^{-1}), then 20 mL of deionized water was added dropwise to the above mixture under vigorous stirring. After 30 min, the mixture was filtered and dried at 100 °C, then calcined in air at 500 °C for 5 h at a heating rate of 2 °C/min. The obtained sample was labeled as TiO_2/Cr-MCM-41, in which the molar ratio of Ti:Si is also 0.03.

2.2. Characterization

X-ray diffraction patterns (XRD) of the synthesized photocatalysts were obtained from a PANalytical X'pert MPD Pro diffractometer using Ni-filtered Cu Kα irradiation (wavelength 1.5406 Å). N_2 adsorption–desorption isotherms of photocatalysts were conducted at 77 K in the Beckman Coulter SA3100 plus instrument. Samples were degassed at 300 °C for 60 min, prior to measurements. Surface area was determined using the Brunauer–Emmett–Teller (BET) methods. Elemental analysis was conducted on the Bruker S4 PIONEER X-ray fluorescence spectrum (XRF) using Ru target and 4 kW maximum power. Diffuse reflectance UV–vis spectra (UV–vis) of the photocatalysts were measured on a HITACHI U4100 instrument equipped with labsphere diffuse reflectance accessory. Fourier transform infrared spectra (FTIR) were recorded on a Nicolet AVATAR 360 FTIR spectrometer using the KBr pellet technique. Raman scattering study was performed on the Jobin Yvon LabRAM HR Spectrometer with 514.5 nm irradiation from an argon ion laser at 20 mW.

2.3. Evaluation of photocatalytic activity

The photocatalytic activities of the samples were examined in a gas-closed system. Typically, 0.2 g of catalyst powder was dispersed in a Pyrex reaction cell containing 200 mL aqueous formic acid solution (in the volume of H_2O:HCOOH = 3:1). Before light irradiation, the photoreaction system was purged with N_2 for 30 min to remove air. The reaction was performed under vigorous stirring using a magnetic stirring rod coated with polytetrafluoroethylene (PTFE). The light source was a 350-W Xe lamp equipped with an optical cutoff filter ($\lambda > 430$ nm). A shutter window and a water filter were placed between the Xe lamp and the reaction cell to remove infrared (IR) light illumination. The amount of the H_2 produced was analyzed in situ by gas chromatography (NaX zeolite column, TCD detector, nitrogen as carrier gas). Blank experiments revealed that no hydrogen was produced without catalyst or light irradiation.

3. Results and discussion

3.1. FTIR

The FTIR spectra of Cr(x)-MCM-41 and Cr(x)-Ti-MCM-41 are shown in Fig. 1. In all the samples a FTIR band around 960 cm^{-1} is observed, which is often assigned to a lattice defect and is correlated with the presence of chromium ions (or other framework ions such as Ti) in a chromium silicate-1 framework. This 960 cm^{-1} band is also prominent in the FTIR spectrum of the pure siliceous MCM-41. By carefully examining this band, it is at 967 cm^{-1} in siliceous MCM-41 and red shifted slightly with an increase in the amount of incorporated Cr, which may be due to an interaction between the Cr atoms and silicon (forming Cr–O–Si bonds) [12] suggesting that the atom Cr has been incorporated into the framework of MCM-41. Another band at about 1640 cm^{-1} was assigned to Si–OH vibrations. A broad band at about 1090 cm^{-1}, with a shoulder at 1250 cm^{-1}, and a band at 808 cm^{-1}, corresponded to asymmetric and symmetric Si–O stretching vibrations, respectively [13].

3.2. N_2 adsorption–desorption isotherms

The N_2 adsorption–desorption isotherms of Cr(x)-MCM-41 and Cr(x)-Ti-MCM-41 are depicted in Fig. 2. A type IV adsorption isotherm typical of mesoporous solids is observed for all the samples [14], except for x = 10. Adsorption at low pressures ($P/P_0 < 0.25$) is accounted for by monolayer–multilayer adsorption of N_2 on the walls of the mesopores. At relative pressure, P/P_0 between 0.25 and 0.45, an inflection due to capillary condensation within the mesopores is observed, which becomes less sharp with the increased amount of incorporated Cr and disappears at x = 10. This result means that the well-ordered mesoporous structure of Cr(x)-MCM-41 and Cr(x)-Ti-MCM-41 could be destroyed by increasing the amount of incorporated Cr.

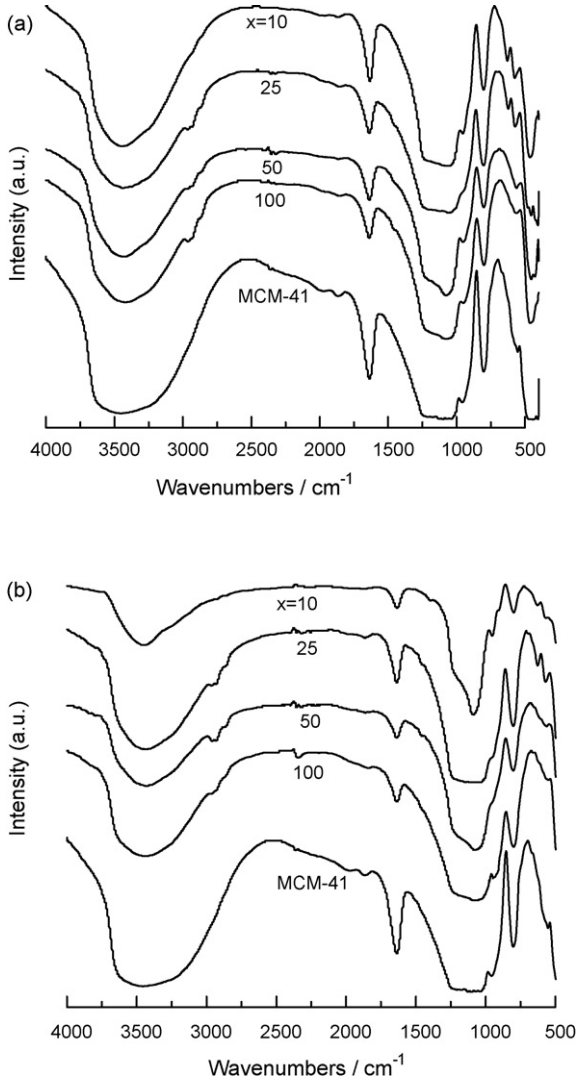

Fig. 1. The FTIR spectra of Cr(*x*)-MCM-41 (a) and Cr(*x*)-Ti-MCM-41 (b).

Low-temperature nitrogen adsorption isotherms enable the measurement of the surface area. When $x = 100$, the surface areas of Cr(*x*)-MCM-41 and Cr(*x*)-Ti-MCM-41 were 979.2 and 823.9 m^2/g, respectively, and decreased continuously with the increasing amount of incorporated Cr (shown in Table 1). This continuous decrease in the surface area with increasing Cr content is similar to Ga- or Al-containing MCM-41 [15,16].

3.3. XRD

Fig. 3 gives out the XRD patterns of Cr(*x*)-MCM-41. Low-angle XRD patterns of Cr(*x*)-MCM-41 ($x = 100$, 50, 25) are consistent with earlier reports [6] indicating a hexagonal structure for these materials, the intensity of the (1 0 0) peak decreases with increasing Cr content, this may be due to the partial structure collapse, which is consistent to the result of N_2 adsorption isotherms. While $x = 10$, we cannot find any peak in the low-angle XRD patterns, which imply that certain amount of Cr-incorporation could destroy Si–O framework and lead to the collapse of the regular order of mesostructured pores. It can also be observed that the unit cell parameter d_{100} spacing

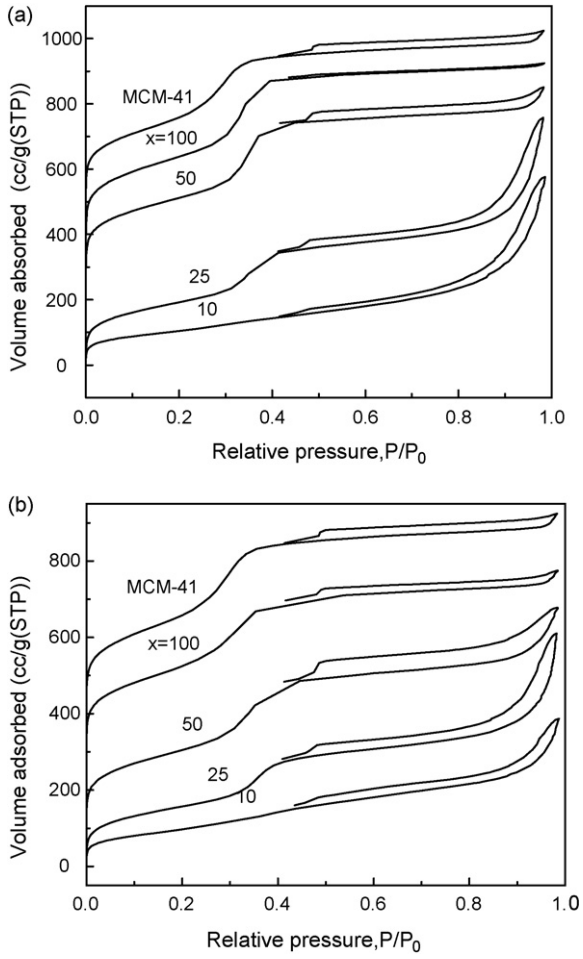

Fig. 2. N_2 adsorption–desorption isotherms of Cr(*x*)-MCM-41(a) and Cr(*x*)-Ti-MCM-41 (b).

slightly increases with increasing Cr content (shown in Table 2), which is similar to Ulagappan and Rao's report [17], indicating that Cr atom had been incorporated into the Si–O framework.

The high-angle XRD patterns of Cr(*x*)-MCM-41 exhibit peak assigned to amorphous silica ($2\theta = 22.5^\circ$) [18], and no other peaks are observed, indicating that the Cr atoms have been highly dispersed into mesoporous framework structure rather than exist as chromium oxides out of the silica framework. However, with increasing Cr content, the peaks assigned to Cr_2O_3 becomes more and more clear, which means that the amount of Cr exceeds the capacity of MCM-41 for

Table 1
XRF analysis results, surface area and rate of hydrogen evolution of the photocatalysts (the data at the left and right to slash "/" belongs to Cr(*x*)-MCM-41 and Cr(*x*)-Ti-MCM-41, respectively)

x (Initial mole rate of Si to Cr)	Final mole rate of Si to Cr	BET surface area (m^2/g)	Rate of hydrogen evolution ($\lambda > 430$ nm) ($\mu mol\ h^{-1}\ g_{Cr}^{-1}$)
100	122/100	979.2/823.9	47.2/146.5
50	56/53	883.3/747.4	9.4/39.7
25	27/27	699.7/521.4	1.7/2.5
10	12/11	377.9/352.9	0/0.8

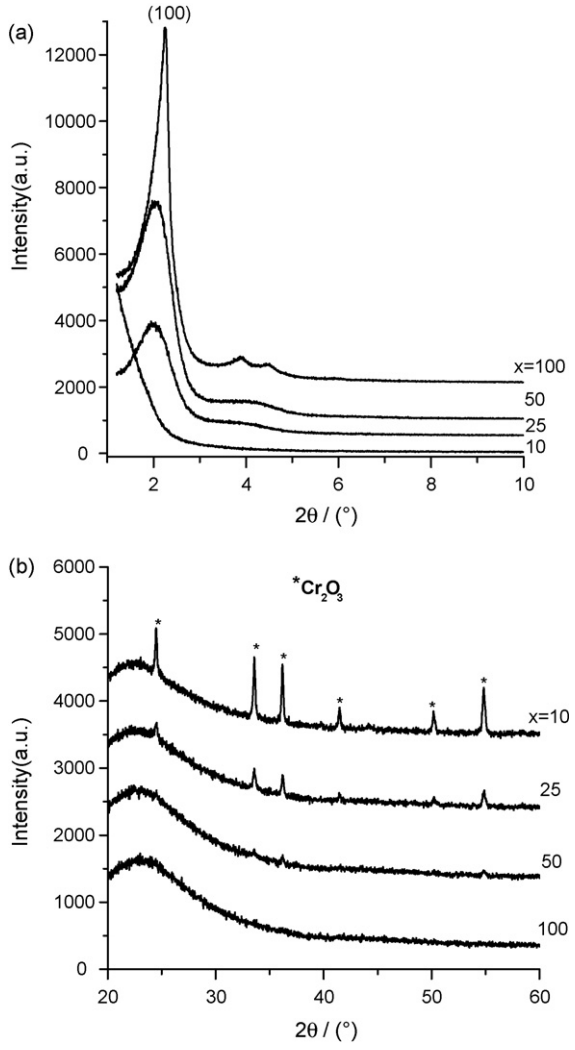

Fig. 3. Low-angle (a) and high-angle (b) XRD patterns of Cr(*x*)-MCM-41.

heterogeneous element incorporation. The XRD patterns of Cr(*x*)-Ti-MCM-41 were similar to those of Cr(*x*)-MCM-41 shown in Fig. 4, except that the intensity of (1 0 0) peak for the later was higher than that of the Cr(*x*)-Ti-MCM-41 with the same Cr content. This is probably because of the destruction of the mesoporous structure of Cr(*x*)-MCM-41 [19]. One cannot find any characteristic peaks assigned to titanium oxide from the high-angle XRD patterns of Cr(*x*)-Ti-MCM-41, which infers that Ti atoms have been highly dispersed into mesoporous framework structure.

Table 2
Textural properties of Cr(*x*)-MCM-41

Material	d_{100} (Å)[a]	a_0 (Å)[b]
Cr(100)-MCM-41	39.25	45.33
Cr(50)-MCM-41	43.29	49.99
Cr(25)-MCM-41	45.06	52.03
Cr(10)-MCM-41	–	–

[a] Calculated from $2d_{100} \sin\theta = \lambda$.
[b] Calculated from $a_0 = 2d_{100}/\sqrt{3}$.

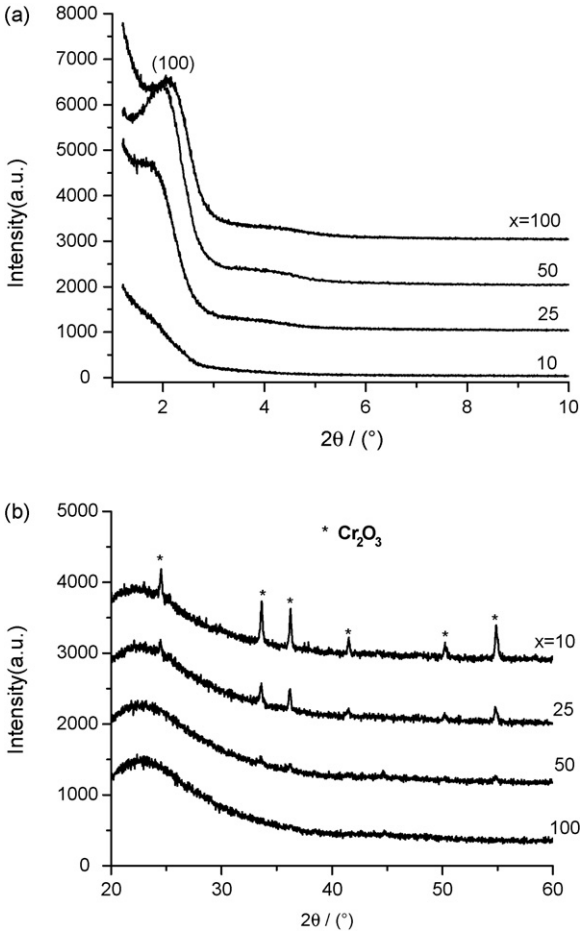

Fig. 4. Low-angle (a) and high-angle (b) XRD patterns of Cr(*x*)-Ti-MCM-41.

3.4. Raman

To further identify the state of Ti in the Cr(*x*)-Ti-MCM-41, the Raman spectra of Cr(100)-Ti-MCM-41 and TiO_2/Cr(100)-MCM-41 are shown in Fig. 5. The molar ratio of Ti:Si in either sample is 0.03. One can easily find three clear bands around 400, 520, 620 cm^{-1}, characteristic for anatase [20], appear in the Raman spectrum of TiO_2/Cr(100)-MCM-41. However, the Raman bands assigned to anatase cannot be observed from the Raman spectrum of Cr(100)-Ti-MCM-41, therefore, the presence of TiO_2 clusters can be excluded. Additionally, a broad Raman band is observed at 919 cm^{-1}. This band has been assigned to silica vibrations perturbed by the presence of Ti, which is indicative of the formation of Si–O–Ti bonds [21]. These are strong evidences for the titanium atoms incorporated into the framework of Cr(100)-Ti-MCM-41.

3.5. UV–vis

Fig. 6(a and b) show UV–vis absorption spectra for Cr(*x*)-MCM-41 and Cr(*x*)-Ti-MCM-41, respectively. For all the samples, a broad peak at 610 nm, characteristic of Cr^{3+} has been seen. This peak can be assigned to the d–d transitions [12,22]. The band is assigned to $^4A_{2g} \rightarrow {}^4T_{1g}$ transitions. The transition can be due to Cr_2O_3 or isolated Cr^{3+} ions. However,

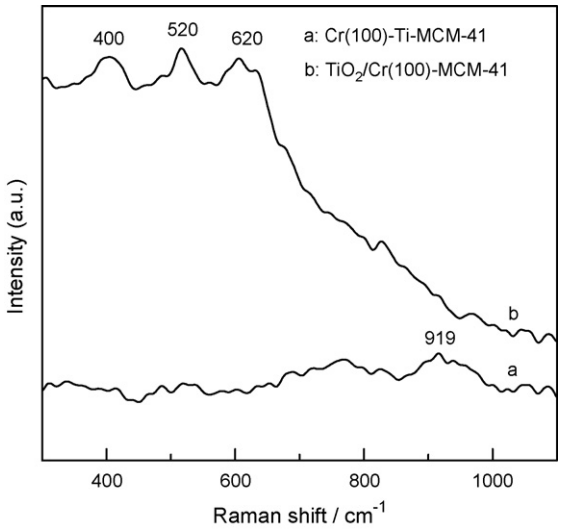

Fig. 5. Raman spectra of Cr(100)-Ti-MCM-41 and TiO_2/Cr(100)-MCM-41.

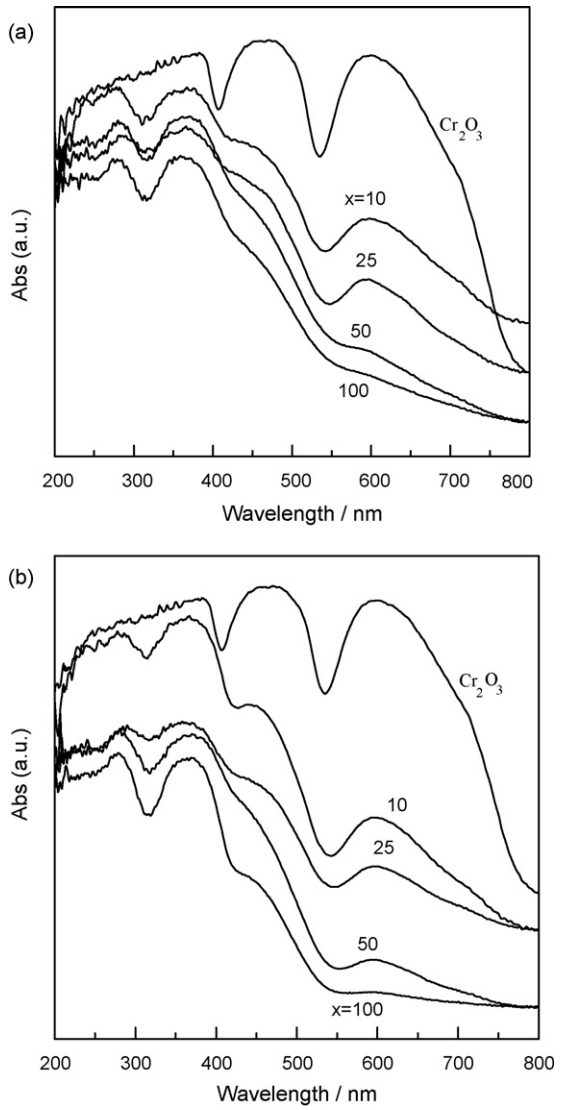

Fig. 6. UV–vis spectra of Cr(x)-MCM-41 (a) and Cr(x)-Ti-MCM-41 (b).

for the samples with $x = 100$, the absence of any peaks in the XRD due to Cr_2O_3 suggests that the Cr^{3+} ions are well dispersed and isolated in the framework. The UV–vis spectrum of all the samples show bands at 275 and 350 nm and a shoulder at 440 nm, which most likely represent the $O^{2-} \rightarrow Cr^{6+}$ charge transfer absorption bands [23]. However, d–d transition of Cr^{5+} occurs in the same spectral region [24].

3.6. Photocatalysis

Fig. 7(a and b) respectively shows the H_2 evolution from water over Cr-MCM-41 and Cr-Ti-MCM-41 under visible light ($\lambda > 430$ nm) irradiation. During the 18-h reaction period, the hydrogen evolution rate did not decrease as the reaction proceeded, which means that the photocatalysts are stable and long-lived with HCOOH as the sacrificial agent. From Table 1, we can see that the final mole rate of Si to Cr is higher than the initial rate x, meaning that some of Cr leached during the hydrothermal procedure. Also we can observe that, with the same initial mole rate of Si to Cr, the final mole rate of Si to Cr in Cr-Ti-MCM-41 is less than that in Cr-MCM-41. This may be attributed to the co-incorporation of Ti along with Cr into MCM-41, as the incorporated Ti atoms linked to Cr atoms by an oxo bridge, hence preventing Cr leaching. With increasing Cr

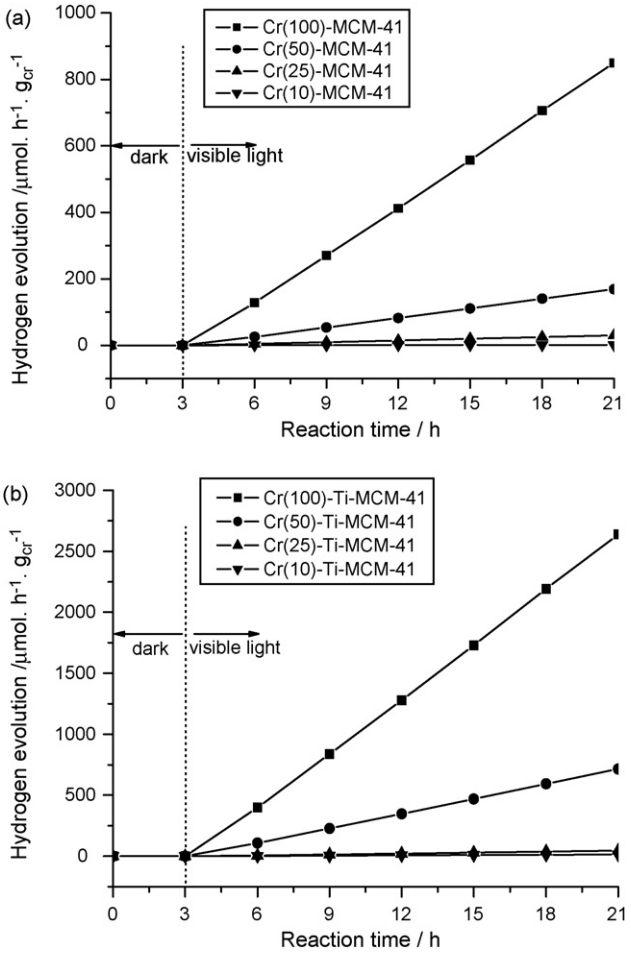

Fig. 7. H_2 evolution over Cr-MCM-41 (a) and Cr-Ti-MCM-41 (b) under visible light irradiation.

content, the BET surface area of Cr(x)-MCM-41 and Cr(x)-Ti-MCM-41 decreases, so does the rate of hydrogen evolution. From these results, we can deduce that the increasing content of Cr partly builds up the mesoporous channel and weakens the order of the mesoporous structure, which results in the decrease of photocatalytic active sites, hence the lower rate of hydrogen evolution. Compared with the Cr-MCM-41 which has the same amount of incorporated Cr, the Cr-Ti-MCM-41 exhibits much higher hydrogen evolution activity. This may be related to the different charge transfer mechanisms for Cr-MCM-41 [8] and Cr-Ti-MCM-41 [25], respectively.

For Cr(x)-MCM-41, these highly dispersed chromium ions can be excited under visible-light irradiation to form the corresponding charge-transfer excited state involving an electron transfer from O^{2-} to Cr^{6+} as shown by $[Cr^{6+}-O^{2-}] \xrightarrow{h\upsilon} [Cr^{5+}-O^{-}]^{*}$ [8]. These charge-transfer excited states have high reactivity due to the presence of electron–hole pairs localized next to each other, compared with electron–hole pairs produced in traditional semiconductors such as TiO_2, ZnO, or CdS [26]. Thus, the localized electron–hole pairs under visible-light irradiation initiate unique photocatalytic activities that cannot usually be found on dispersed metal oxide semiconductors. The hole produced by excitation can react with the surface hydroxyl groups on the surfaces of Cr(x)-MCM-41 [27] to form hydroxyl radicals which can further react with the electron donors HCOOH. Thus, the electrons in the localized electron–hole pairs $[Cr^{5+}–O^{-}]^{*}$ reduce H^{+} to generate H_2. After the electron and hole reacts with H^{+} and HCOOH, respectively, the localized pairs $[Cr^{5+}–O^{-}]^{*}$ turned back to be $[Cr^{6+}–O^{2-}]$, that is to say, the Cr^{6+} in the catalysts would not be reduced to low oxidation state such as Cr^{3+}, which can also be proved by our 18-h photocatalytic reaction (Fig. 7) without any decrease in activity, meaning that these photocatalysts are stable. However, the photocatalytic activity will decrease with the amount of incorporated Cr increases. Use of Cr_2O_3 as a catalyst does not exhibit photocatalytic hydrogen evolution, suggesting that polymerized Cr^{3+} species are inactive for photocatalytic hydrogen evolution [28]. The low activity of Cr-MCM-41 with higher Cr content can thus be attributed to the formation of Cr^{3+} species on the photocatalysts, as well as that the decreased surface area lessens the photoactive sites.

Because of the presence of Ti in the framework of Cr(x)-Ti-MCM-41, the photocatalytic mechanism of Cr(x)-Ti-MCM-41 is different from that of Cr(x)-MCM-41. Lin and Frei [25] have reported that engaging a second metal center as a donor linked to the first metal by an oxo bridge may offer a robust chromophore, which was described as oxo-bridged metal-to-metal charge-transfer (MMCT) mechanism. Considering the co-incorporation of Cr and Ti in Cr(x)-Ti-MCM-41, we can deduce that the formed interaction (Cr–O–Ti) [25,29] has a good correlation with the catalyst's photocatalytic activity [30,31]. The photoexcited localized electron–hole pairs formed in Cr(x)-Ti-MCM-41 also have high reactivity as in Cr(x)-MCM-41, and more importantly, the nature of the Ti center linked to Cr center via oxo bridge (Cr–O–Ti) suppresses the electron–hole recombination to a larger extent, compared to Cr(x)-MCM-41, which has only one single metal center. This explains the reason why the Cr(x)-Ti-MCM-41 has higher photocatalytic activity for hydrogen evolution than Cr(x)-MCM-41 when the amount of incorporated Cr is the same.

4. Conclusions

In conclusion, we have successfully prepared a series of Cr incorporated and Cr, Ti co-incorporated MCM-41 photocatalysts by a simple hydrothermal procedure. FTIR analysis indicated that the well dispersion of the element Cr in the framework of the mesoporous structure with negligible bulk oxide formation when the amount of incorporated Cr was rather low (such as mole rate of Si/Cr = 100), while combined results of XRD, N_2 adsorption–desorption isotherms and UV–vis absorption spectrum proved that the mesoporous structure of Cr-MCM-41 and Cr-Ti-MCM-41 photocatalysts could be destroyed with an increase in the amount of incorporated Cr, which resulted in the low rate of hydrogen evolution under visible light irradiation ($\lambda \geq 430$ nm). The results of photocatalytic tests also presented that the Cr-Ti-MCM-41 exhibited much higher hydrogen evolution activity than the Cr-MCM-41 with the same amount of incorporated Cr, which could be explained by their different charge transfer mechanisms.

Acknowledgements

The authors gratefully acknowledge the financial supports of the National Natural Science Foundation of China (No. 50521604) and National Basic Research Program of China (No. 2003CB214500).

References

[1] K. Sunada, Y. Kikuchi, K. Hashimoto, A. Fujishima, Environ. Sci. Technol. 32 (1998) 726.
[2] A.Y. Nosaka, T. Fujiwara, H. Yagi, H. Akutsu, Y. Nosaka, Langmiur 19 (2003) 1935.
[3] H. Kato, A. Kudo, J. Phys. Chem. B 106 (2002) 5029.
[4] K. Sayama, H. Arakawa, J. Phys. Chem. 97 (1993) 531.
[5] C.T. Kresge, M.E. Leonowicz, W.J. Roth, J.C. Vartuli, J.S. Beck, Nature 359 (1992) 710.
[6] J.S. Beck, J.C. Vartuli, W.J. Roth, M.E. Leonowicz, C.T. Kresge, K.D. Schmitt, C.T.W. Chu, D.H. Olson, E.W. Sheppard, S.B. McCullen, J.B. Higgins, J.L. Schlenker, J. Am. Chem. Soc. 114 (1992) 10834.
[7] S. Zhang, L. Gao, Q. Zhang, W. Zhang, J. Guo, J. Mater. Chem. 11 (2001) 578.
[8] S. Rodrigues, K.T. Ranjit, S. Uma, I.N. Martyanov, K.J. Klabunde, J. Catal. 230 (2005) 158.
[9] S. Rodrigues, S. Uma, I.N. Martyanov, K.J. Klabunde, J. Photochem. Photobiol. A: Chem. 165 (2004) 51.
[10] S.H. Liu, H. Wang, Y.J. Huang, Y.M. Sun, K.S. Lin, M.C. Hsiao, Energy Sources 25 (2003) 591.
[11] L.Z. Wang, J.L. Shi, J. Yu, D.S. Yan, Nanostruct. Mater. 10 (1998) 1289.
[12] Z. Zhu, Z. Chang, L. Kevan, J. Phys. Chem. B 103 (1999) 2680.
[13] Y. Kong, H. Zhu, G. Yang, X. Guo, W. Hou, Q. Yan, M. Gu, C. Hu, Adv. Funct. Mater. 14 (2004) 816.
[14] K.S.W. Sing, D.H. Evrett, R.A.W. Haul, L. Moscou, Pure Appl. Chem. 57 (1985) 603.
[15] C. Cheng, H. He, W. Zhou, J. Klinowski, J. Goncalves, L. Gladden, J. Phys. Chem. 100 (1996) 390.

[16] Z. Luan, H. He, W. Zhou, C. Cheng, J. Klinowski, J. Chem. Soc., Faraday Trans. 91 (1995) 2955.
[17] N. Ulagappan, C.N.R. Rao, Chem. Commun. 9 (1996) 1047.
[18] Y. Shan, L. Gao, S. Zhang, Mater. Chem. Phys. 88 (2004) 192.
[19] V. Parvulescu, C. Anastasescu, B.L. Su, J. Mol. Catal. A: Chem. 211 (2004) 143.
[20] K. Cassiers, T. Linssen, M. Mathieu, Y.Q. Bai, H.Y. Zhu, P. Cool, E.F. Vansant, J. Phys. Chem. B 108 (2004) 3713.
[21] X. Gao, S.R. Bare, J.L.G. Fierro, M.A. Banares, I.E. Wachs, J. Phys. Chem. B 102 (1998) 5653.
[22] B.M. Weckhuysen, I.E. Wachs, R.A. Schoonheydt, Chem. Rev. 96 (1996) 3327.
[23] H. Yamashita, K. Yoshizawa, M. Ariyuki, S. Higashimoto, M. Che, M. Anpo, Chem. Commun. 5 (2001) 435.
[24] C.D. Garner, J. Kendrick, P. Lambert, F.E. Maabs, I.H. Hiller, Inorg. Chem. 15 (1976) 1287.
[25] W. Lin, H. Frei, J. Phys. Chem. B 109 (2005) 4929.
[26] M. Matsuoka, M. Anpo, J. Photochem. Photobiol. C: Photochem. Rev. 3 (2003) 225.
[27] X.S. Zhao, G.Q. Lu, A.J. Whittaker, G.J. Millar, H.Y. Zhu, J. Phys. Chem. B 101 (1997) 6525.
[28] J. Wang, S. Uma, K.J. Klabunde, Appl. Catal. B: Environ. 48 (2004) 151.
[29] E.P. Reddy, L. Davydov, P.G. Smirniotis, J. Phys. Chem. B 106 (2002) 3394.
[30] S. Rodrigues, K.T. Ranjit, S. Uma, I.N. Martyanov, K.J. Klabunde, Adv. Mater. 17 (2005) 2467.
[31] B. Sun, E.P. Reddy, P.G. Smirniotis, Appl. Catal. B: Environ. 57 (2005) 139.